



Dalton  
Transactions

**Syntheses and Characterizations of Iron Complexes of Bulky  
o-Phenylenediamide ligand**

Journal:	<i>Dalton Transactions</i>
Manuscript ID	DT-ART-06-2020-002087.R2
Article Type:	Paper
Date Submitted by the Author:	12-Aug-2020
Complete List of Authors:	Liang, Qiuming; University of Toronto, Department of Chemistry Lin, Jack; University of Toronto, Department of Chemistry DeMuth, Joshua; University of Rochester, Department of Chemistry Neidig, Michael; University of Rochester, Chemistry Song, Datong; University of Toronto, Department of Chemistry

SCHOLARONE™  
Manuscripts

## ARTICLE

## Syntheses and Characterizations of Iron Complexes of Bulky *o*-Phenylenediamide ligand

Qiuming Liang,<sup>a</sup> Jack H. Lin,<sup>a</sup> Joshua C. DeMuth,<sup>b</sup> Michael L. Neidig<sup>b</sup> and Datong Song<sup>\*a</sup>

Received 00th January 20xx,  
Accepted 00th January 20xx

DOI: 10.1039/x0xx00000x

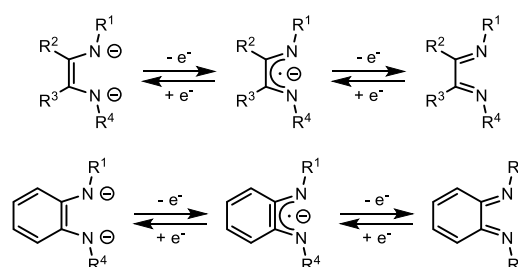
We report the syntheses of a family of tetrahedral iron complexes bearing a bulky redox active *o*-phenylenediamide ligand. The electronic structures of these complexes have been investigated by Mössbauer spectroscopy, magnetic susceptibility measurements, and X-ray crystallography.

### Introduction

Within the last decade, redox-active ligands have attracted considerable attention, owing to their unusual and intriguing electronic structures.<sup>1</sup> Redox-active ligands have more energetically accessible levels for reduction or oxidation.<sup>1</sup> Their coordination to metal centres induces radical reactivity and electron reservoir behaviour, which is often utilized to develop exciting catalytic activities.<sup>1–3</sup> The oxidation level of the redox-active ligands in complexes can be determined by high-quality X-ray crystallography, a broad set of spectroscopic methods, and density functional theory (DFT) calculations. A combination of a redox active metal, such as iron, with redox-active ligands can lead to unique chemical and magnetochemical properties. In these cases, the determination of the oxidation state of the transition-metal ion is not straightforward. For instance, a ferric ion in such species may adopt a high-, intermediate-, or low-spin electronic configuration ( $S_{\text{Fe}} = 5/2, 3/2, \text{ or } 1/2$ , respectively;  $S$  is the total spin quantum number), whereas a ferrous ion may also have high-, intermediate-, and low-spin electronic configurations ( $S_{\text{Fe}} = 2, 1, \text{ or } 0$ , respectively). Strong intramolecular antiferromagnetic coupling of a radical ligand or a second metal centre may yield a large variety of different spin ground states.

$\alpha$ -Diimines and *o*-phenylenediamides (pda) are classic examples of redox-active ligands that form five-membered chelate rings with a large variety of transition and main-group elements.<sup>4–6</sup> It has been clearly established that  $\alpha$ -diimines and pda ligands each exist in three different redox forms in coordination compounds, including a closed-shell dianion ( $S =$

0), an open-shell  $\pi$  radical monoanion ( $S = 1/2$ ), and a closed-shell neutral ( $S = 0$ ) form (Scheme 1).<sup>4</sup> Iron complexes based on  $\alpha$ -diimine ligands including 1,4-diaza-1,3-butadiene (dad) and bis(imino)acenaphthene (BIAN) were widely investigated.<sup>7–9</sup> Furthermore, iron complexes of  $\alpha$ -diimine ligands are efficient catalysts for the hydrogenation of alkenes,<sup>8a,9a</sup> hydrovinylation of dienes,<sup>8b</sup> (cyclo)dimerization of dienes,<sup>8c–e</sup> cyclotrimerization of alkynes,<sup>8f</sup> Diels–Alder type cycloaddition of dienes with alkynes,<sup>8f</sup> dehydrogenation of amine–boranes,<sup>8g</sup> and hydrosilylation of carbonyls.<sup>9b,c</sup>



**Scheme 1.** Different redox states of  $\alpha$ -diimine and *o*-phenylenediamide (pda) derived ligands.

In contrast to iron  $\alpha$ -diimine complexes, iron pda complexes are relatively less studied. Wiegardt and co-workers have reported several homoleptic pda iron complexes and dad–pda heteroleptic iron complexes, which displayed sophisticated electronic structures.<sup>7</sup> Hernán-Gómez and Costas have recently reported the reactivity of  $[\text{Fe}(\text{C}^{6\text{F}_5}\text{pda})(\text{THF})_2]$  ( $\text{C}^{6\text{F}_5}\text{pda} = N,N'$ -bis(pentafluorophenyl)-*o*-phenylenediamido-) toward the intramolecular  $\text{C}(sp^3)\text{–H}$  activation of diazoesters in the presence of  $\text{LiAl}[\text{OC}(\text{CF}_3)_3]_4$  under mild reaction conditions, yielding a variety of carbocyclic cyclopentanes as well as bicyclic spiro and fused ring compounds.<sup>7f</sup> Our group has reported the  $[\text{Fe}^{\text{I}}(\text{Dipp}^{\text{pda}^-})(\text{toluene})]$  ( $\text{Dipp}^{\text{pda}} = N,N'$ -bis(2,6-diisopropylphenyl)-*o*-phenylenediamido-) and  $[\text{Fe}^{\text{0}}(\text{Dipp}^{\text{pda}^0})(\text{CO})_3]$  complexes.<sup>7g</sup> We herein report the synthesis of a series of iron compounds supported by the  $\text{Dipp}^{\text{pda}}$  ligand platform at various oxidation

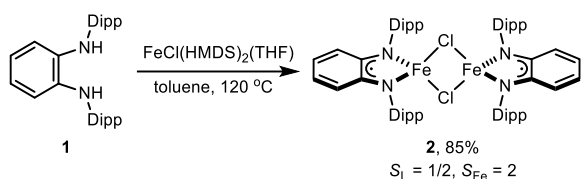
<sup>a</sup> Davenport Chemical Research Laboratories, Department of Chemistry, University of Toronto, 80 St. George Street, Toronto, Ontario, Canada, M5S 3H6.

<sup>b</sup> Department of Chemistry, University of Rochester, Rochester, New York, USA, 14627.

E-mail: [d.song@utoronto.ca](mailto:d.song@utoronto.ca)

† Electronic supplementary information (ESI) available: NMR and Mössbauer spectra and X-ray crystallographic experimental details. CCDC 2009196–2009200, 2009218 and 2022767–2022770. For ESI and crystallographic data in CIF or other electronic format see DOI: 10.1039/x0xx00000x.

states. Spectroscopic data as well as X-ray crystallographic analysis are used to characterize this series of new complexes.



Scheme 2. Synthesis of compound 2.

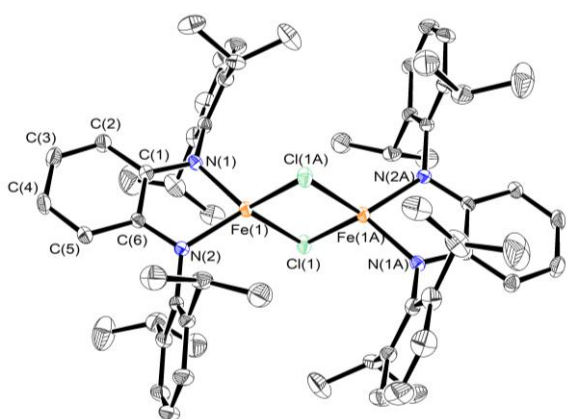


Figure 1. Molecular structure of **2** (30% probability thermal ellipsoids). All hydrogen atoms are omitted for clarity.

## Results and Discussion

Reacting  $\text{Dipp-pdaH}_2$  (**1**) with  $[\text{FeCl}(\text{HMDS})_2(\text{THF})]$  (HMDS = hexamethyldisilazide) in toluene at 120 °C gives complex **2** in good yields (Scheme 2). The use of bulky Dipp substituents is important, as smaller pda ligands tend to form  $[\text{Fe}(\text{pda})_2]$ .<sup>7</sup> The  $^1\text{H}$  NMR spectrum of complex **2** in  $\text{C}_6\text{D}_6$  at 25 °C shows paramagnetically shifted and broadened resonances between +159 and –15 ppm. X-ray crystallographic analysis of **2** revealed a dinuclear structure with a crystallographically imposed inversion centre (Figure 1). The bond lengths within the  $\text{Dipp-pda}$  ligands reveal a quinoid-type distortion. The C(1)–N(1) and C(6)–N(2) bond lengths are 1.341(2) and 1.346(2) Å (Table 1), respectively, in between the typical C–N single and double bond lengths. The  $\text{C}_\alpha$ – $\text{C}_\alpha'$  and  $\text{C}_\gamma$ – $\text{C}_\gamma'$  bond lengths are 1.452(2) and 1.405(3) Å, respectively, while the other four bonds of the phenylene backbone feature the long  $\text{C}_\alpha$ – $\text{C}_\beta$  and  $\text{C}_\alpha$ – $\text{C}_\beta'$  bonds (1.419(2) and 1.421(2) Å) and short  $\text{C}_\beta$ – $\text{C}_\gamma$  and  $\text{C}_\beta$ – $\text{C}_\gamma'$  bonds (1.363(3) and 1.361(3) Å). The pattern in these metric parameters suggests that the pda ligands are open-shell  $\pi$  radical anions, i.e.,  $\text{Dipp-pda}^{\cdot-}$  ( $S = 1/2$ ).<sup>4</sup> As such, the iron centres are Fe(II) to balance the charge. The Fe(1)–N(1) and Fe(1)–N(2) bond lengths are 1.979(2) and 1.977(1) Å, respectively, suggesting that the Fe<sup>II</sup> centres are high-spin, i.e.,  $S_{\text{Fe}} = 2$ . The intramolecular Fe–Fe distance of 3.0255(4) Å in **2** is considerably longer than the sum of the covalent radii (2.50 Å), making it outside of the range of Fe–Fe bonds.<sup>10</sup> The Fe–Fe distance is slightly longer than that found in  $[\text{Fe}(\mu_2\text{-Cl})(\text{Dippdad})_2]$  (2.9764(6) Å,  $\text{Dippdad} = N,N'$ -bis-(2,6-diisopropylphenyl)-2,3-dimethyl-1,4-diaza-1,3-butadiene),<sup>7a,b</sup> suggesting an even weaker exchange

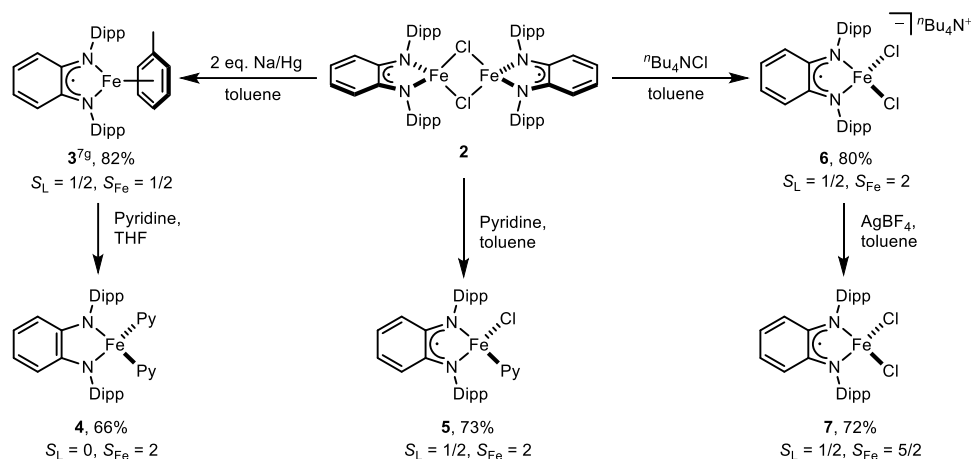
coupling between the two iron centres. The solution magnetic moment of **2** is 5.4  $\mu_{\text{B}}$  in  $\text{C}_6\text{D}_6$  at 25 °C (Table 2), while  $[\text{Fe}(\mu_2\text{-Cl})(\text{Dippdad})_2]$  was reported to have solution<sup>7a</sup> magnetic moment of 3.86  $\mu_{\text{B}}$ . The greater solution magnetic moment of compound **2** compared to that of  $[\text{Fe}(\mu_2\text{-Cl})(\text{Dippdad})_2]$  is likely due to a weaker antiferromagnetic coupling between the two iron centres in **2**.

Zero-field  $^{57}\text{Fe}$  Mössbauer spectroscopy was used to examine the oxidation state and spin state of the iron centres of complex **2** (Table 2). The Mössbauer spectrum of complex **2** at 80 K features one doublet with an isomer shift ( $\delta$ ) of 0.84 mm/s and a quadruple splitting ( $|\Delta E_{\text{Q}}|$ ) of 3.64 mm/s (Figure S10), typical for high-spin Fe<sup>II</sup> species.<sup>7c,11</sup> Such a spectrum suggests that the two high-spin ferrous centres are equivalent, consistent with the crystallographic data. Overall, the experimental data are consistent with an electronic structure with strong antiferromagnetic coupling within each  $\text{Dipp-pda}^{\cdot-}$ –Fe<sup>II</sup> pair and weak coupling between the two iron centres across the bridging chloride ligands.<sup>12</sup>

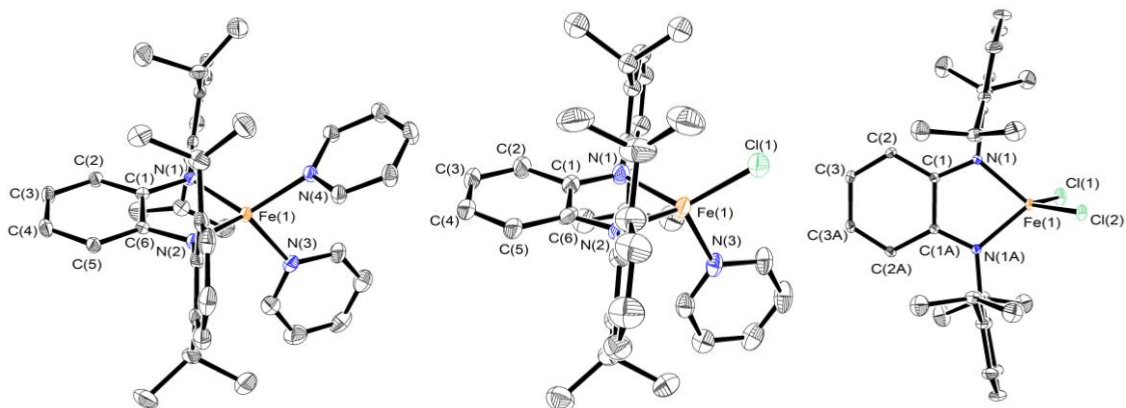
With complex **2** in hand, we set to reduce the metal centre to low valence, hoping for dinitrogen binding. Compound **2** can be reduced with two equivalents of 0.5% sodium amalgam to afford the diamagnetic complex **3** (Scheme 3), featuring a low-spin Fe(I) centre and a  $\text{Dipp-pda}^{\cdot-}$  ligand with strong antiferromagnetic coupling in between.<sup>7b</sup> Attempts to reduce complex **2** in non-arene solvents were not fruitful. The reduced product is able to capture the trace amount of arene vapour in the glovebox atmosphere to give  $[\text{Fe}(\text{Dipp-pda})(\eta^6\text{-arene})]$ , which prevents dinitrogen from binding. The Mössbauer spectrum of **3** (Table 2) features a doublet with an isomer shift of 0.37 mm/s, typical for a low spin ( $S_{\text{Fe}} = 1/2$ ) Fe(I) centre,<sup>11</sup> and a quadrupole splitting of 0.79 mm/s (Figure S11). While the isomer shift is similar to the analogous Fe(<sup>Xyl</sup>dad)( $\eta^6$ -toluene) ( $\delta = 0.44$  mm/s,  $|\Delta E_{\text{Q}}| = 0.41$  mm/s)<sup>8h</sup> and Fe(<sup>Dipp</sup>BIAN)( $\eta^6$ -toluene) ( $\delta = 0.45$  mm/s,  $|\Delta E_{\text{Q}}| = 0.41$  mm/s),<sup>9j</sup> the quadruple splitting is slightly larger.

Previously we showed that replacing the  $\eta^6$ -toluene ligand in **3** with three stronger charge-neutral  $\pi$ -acceptor CO ligands resulted in the formation of the  $[\text{Fe}(\text{pda})(\text{CO})_3]$  where pda is in its charge neutral form and oxidation state of the iron centre is zero, i.e., shift from  $(\text{Dipp-pda}^{\cdot-})\text{Fe}^{\text{I}}$  to  $(\text{Dipp-pda}^0)\text{Fe}^0$ .<sup>7g</sup> We reason that if we replace the  $\eta^6$ -toluene ligand with charge-neutral  $\sigma$ -donor ligands instead, we may be able to achieve the opposite, i.e., shift from  $(\text{Dipp-pda}^{\cdot-})\text{Fe}^{\text{I}}$  to  $(\text{Dipp-pda}^{2-})\text{Fe}^{\text{II}}$ . The addition of two or more equivalents of pyridine to a THF solution of **3** affords a four-coordinate complex **4** (Scheme 3). The X-ray crystal structure of **4** shows a distorted tetrahedral coordination geometry of the iron centre (Figure 2). The C(1)–N(1) and C(6)–N(2) bond lengths are 1.392(3) and 1.399(3) Å (Table 1), respectively, which are close to a typical C–N single bond length. The  $\text{C}_\alpha$ – $\text{C}_\alpha'$  and  $\text{C}_\gamma$ – $\text{C}_\gamma'$  bond lengths are 1.430(3) and 1.367(4) Å, respectively, while the other bond lengths of the phenylene backbone are more even, i.e., within the range of 1.388(4)–1.397(4) Å. Although a crystal structure with a higher resolution is preferable (i.e., to see whether the  $\text{C}_\gamma$ – $\text{C}_\gamma'$  bond length is significantly different from the  $\text{C}_\beta$ – $\text{C}_\gamma$  and  $\text{C}_\beta$ – $\text{C}_\gamma'$  bonds), the current metric parameters suggest that the  $N,N$ -chelating ligand

## ARTICLE



Scheme 3. Syntheses of complexes 3–7.

Figure 2. Molecular structure of **4**, **5** and **7** (30% probability thermal ellipsoids). All hydrogen atoms are omitted for clarity

is a closed-shell dianion  $\text{Dipp}^-\text{pda}^{2-}$  ( $S = 0$ ). To balance the overall charge, the iron centre is a ferrous ion. The solution magnetic moment of **4** is  $5.2 \mu_B$  in  $\text{THF-}d_8$  at  $25^\circ\text{C}$  (Table 2), suggesting a high-spin  $\text{Fe}^{\text{II}}$ . Complex **4** exhibits isomer shift of  $0.72 \text{ mm/s}$  and large quadrupole splitting of  $4.02 \text{ mm/s}$  (Table 2, Figure S12). These values are characteristic for high-spin ferrous species ( $S_{Fe} = 2$ ),<sup>7c,11</sup> corroborating with the crystallographic data and solution magnetic moment. The dissolution of **4** in arene solvents results the immediate formation of  $[\text{Fe}(\text{Dipp}^-\text{pda})(\eta^6\text{-arene})]$  complexes accompanied by a colour change from blue–purple to intense red–purple. The nature of the auxiliary ligand on iron clearly plays a key role on the electronic structure of the pda–Fe moiety.

In comparison, we examined the ligand substitution reactions of **2**, which has a  $(\text{Dipp}^-\text{pda}^{\bullet-})\text{Fe}(\text{II})$  moiety to find out whether we could achieve the electron shift between the pda

ligand and the iron centre by using different auxiliary ligands. The reaction of 2.5 equivalents of pyridine with **2** in toluene affords the four-coordinate complex **5** (Scheme 3). The X-ray crystal structure of **5** reveals a distorted tetrahedral coordination geometry at the iron centre. The  $\text{Fe}(1)\text{--N}(1)$  and  $\text{Fe}(1)\text{--N}(2)$  bond lengths of  $1.995(3)$  and  $2.018(3) \text{ \AA}$  (Table 1) suggest a high-spin  $\text{Fe}^{\text{II}}$  ( $S_{Fe} = 2$ ) centre. The C–C and C–N bond lengths of the pda ligand of **5** and the Mössbauer parameters ( $\delta = 0.81 \text{ mm/s}$ ,  $|\Delta E_Q| = 2.05 \text{ mm/s}$ , Table 2) are similar to those of **2**, suggesting a  $\pi$  radical anion  $\text{Dipp}^-\text{pda}^{\bullet-}$  ( $S = 1/2$ ). The solution magnetic moment of **5** is  $4.2 \mu_B$  in  $\text{C}_6\text{D}_6$  at  $25^\circ\text{C}$  (Table 2), suggesting strong antiferromagnetic coupling between the high-spin ferrous centre ( $S_{Fe} = 2$ ) and the  $\pi$  radical anionic ligand ( $S = 1/2$ ).

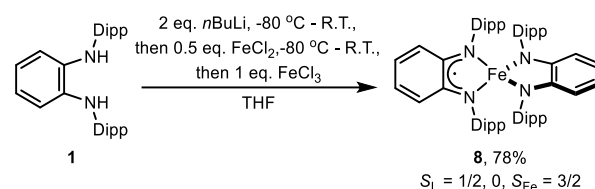
Unable to push an electron from  $\text{Fe}(\text{II})$  into  $\text{Dipp}^-\text{pda}^{\bullet-}$  with the charge-neutral pyridine ligand, we turned to the anionic  $\pi$ -donor chloride ligand. The addition of excess tetrabutylammonium chloride

(5 equiv.) to a toluene solution of **2** at room temperature affords the four-coordinate ferrous salt **6** (Scheme 3). In the solid-state structure of **6**, the C–C and C–N bond lengths of the pda ligand are similar to those of **2**, i.e., a  $\pi$ -radical anion  $\text{Dipp}^{\text{pda}^{\bullet-}}$  ( $S = 1/2$ ). Therefore, the iron centre is assigned as  $\text{Fe}^{\text{II}}$  to balance the charge. The long Fe–N bonds (2.018(2) and 2.003(2) Å) suggest that the  $\text{Fe}^{\text{II}}$  centre in **6** is high-spin. The Mössbauer parameters ( $\delta = 0.80$  mm/s,  $|\Delta E_{\text{Q}}| = 3.04$  mm/s, Table 2) are similar to those of **2** and **5**. The solution magnetic moment of **6** is  $4.1 \mu_{\text{B}}$  in  $\text{C}_6\text{D}_6$  at 25 °C (Table 2), suggesting strong antiferromagnetic coupling between the  $\text{Dipp}^{\text{pda}^{\bullet-}}$  ligand and high-spin  $\text{Fe}^{\text{II}}$  centre.

The anionic  $\pi$ -donor chloride ligand is unable to push an electron from  $\text{Fe}(\text{II})$  into  $\text{Dipp}^{\text{pda}^{\bullet-}}$ , presumably because the  $\text{Dipp}^{\text{pda}^{\bullet-}}$  ligand is not reducing enough. We are curious to know what product we will get if we oxidize complex **6** by  $1e^-$ , i.e.,  $[\text{Fe}^{\text{II}}(\text{Dipp}^{\text{pda}^{\bullet-}})\text{Cl}_2]$  or  $[\text{Fe}^{\text{III}}(\text{Dipp}^{\text{pda}^{\bullet-}})\text{Cl}_2]$ . The reaction of **6** with one equivalent of silver tetrafluoroborate at room temperature in toluene results in a colour change from dark blue–purple to dark green. Compound **7** can be isolated from the reaction mixture as the major product (Scheme 3). The solid-state structure of **7** reveals a  $\text{C}_s$  symmetry and a distorted tetrahedral coordination geometry at the iron centre (Figure 2). The metric parameters of the pda ligand in **7** are similar to those in **2**, **5**, and **6**, i.e.,  $\text{Dipp}^{\text{pda}^{\bullet-}}$ , whereas the Fe–N bonds (1.967(2) Å) in **7** (Table 1) are slightly shorter than those in **2**, **5**, and **6**. The solution magnetic moment of **7** is  $5.1 \mu_{\text{B}}$  in  $\text{C}_6\text{D}_6$  at 25 °C (Table 2). The electronic structure of **7** can be described as  $[\text{Fe}^{\text{III}}\text{Cl}_2(\text{Dipp}^{\text{pda}^{\bullet-}})]$ , with strong antiferromagnetic coupling between the  $\pi$ -radical anion  $\text{Dipp}^{\text{pda}^{\bullet-}}$  ( $S = 1/2$ ) ligand and high-spin ferric ion ( $S = 5/2$ ). The isomer shift and the quadrupole splitting of **7** are 0.39 mm/s and 2.12 mm/s (Table 2, Figure S15), respectively. The reduced isomer shift is consistent with a more oxidized iron centre. In contrast,  $[\text{FeCl}_2(\text{dad})]^{7\text{a,b}}$  and  $[\text{Fe}(\text{DippBIAN})\text{X}_2]^{9\text{j,k}}$  were found to contain  $\text{Fe}^{\text{II}}$  centres and neutral  $N,N$ -chelate ligands. It appears that the  $\text{Dipp}^{\text{pda}^{\bullet-}}$  is less reducing than the corresponding  $\text{DippBIAN}^{\bullet-}$  and  $\text{dad}^{\bullet-}$  ligands. The minor impurity in the sample of **7** displays similar isomer shift and quadrupole splitting to those of **3**, whose formation from the reaction of **6** and  $\text{AgBF}_4$  in toluene could be rationalized as the initial chloride abstraction from **6** by  $\text{Ag}^+$  followed by toluene coordination to the iron centre.

As mentioned above, the bulky Dipp groups are crucial to the synthesis of **2** in minimizing the formation of  $[\text{Fe}(\text{Dipp}^{\text{pda}})_2]$ . In order to prepare the homoleptic complex  $[\text{Fe}(\text{Dipp}^{\text{pda}})_2]$ , **8**, we adopted Wieghardt's synthetic procedures (Scheme 4),<sup>7c</sup> i.e., reacting the doubly deprotonated **1** with  $\text{FeCl}_2$  followed by oxidation with  $\text{FeCl}_3$ . The molecular structure of **8** consists of two chelating  $\text{Dipp}^{\text{pda}}$  ligands bound to a distorted tetrahedral iron centre (Figure 3). The metric parameters of the pda ligands in **8** (Table 1) are in between those of the  $\text{Dipp}^{\text{pda}^{\bullet-}}$  and  $\text{Dipp}^{\text{pda}^{2-}}$  ligands. For example, the C(1)–N(1) and C(6)–N(2) bond lengths are 1.372(3) and 1.376(3) Å, respectively, whereas the corresponding C–N bond lengths in the lithium salts of the  $\text{Dipp}^{\text{pda}^{\bullet-}}$  and  $\text{Dipp}^{\text{pda}^{2-}}$  are 1.341(3) and 1.395(2) Å, respectively. The solution magnetic moment of **8** is  $2.7 \mu_{\text{B}}$  in  $\text{C}_6\text{D}_6$  at 25 °C (Table 2). The crystallographically imposed 2-fold axis relating the two  $\text{Dipp}^{\text{pda}}$  ligands suggests two identical ligands within one molecule of **8**. The electronic structure of a closely related complex  $[\text{Fe}(\text{C}_6\text{F}_5\text{pda})_2]$  was studied in detail by Wieghardt and

co-workers and reported as  $[\text{Fe}^{\text{III}}(\text{C}_6\text{F}_5\text{pda}^{\bullet-})(\text{C}_6\text{F}_5\text{pda}^{2-})]$  with an intermediate-spin  $\text{Fe}^{\text{III}}$  ( $S_{\text{Fe}} = 3/2$ ) antiferromagnetically coupled to a ligand-based radical.<sup>7c</sup> Based on the literature precedence and the available data, we tentatively rationalize the overall electronic structure of **8** using the following major resonance structures  $[\text{Fe}^{\text{III}}(\text{Dipp}^{\text{pda}^{\bullet-}})(\text{Dipp}^{\text{pda}^{2-}})] \leftrightarrow [\text{Fe}^{\text{II}}(\text{Dipp}^{\text{pda}^{2-}})(\text{Dipp}^{\text{pda}^{\bullet-}})]$  in a 1:1 ratio, i.e., a fully delocalized radical over two chelate ligands is antiferromagnetically coupled to an intermediate-spin ferric centre ( $S = 3/2$ ). The Fe–N bond lengths in **8** (1.950(2) and 1.973(2) Å) are longer than those in  $[\text{Fe}^{\text{III}}(\text{C}_6\text{F}_5\text{pda}^{\bullet-})(\text{C}_6\text{F}_5\text{pda}^{2-})]$  (avg. 1.897(3) Å), which could be due to the significantly increased steric congestion associated with the two  $\text{Dipp}^{\text{pda}}$  ligands. Unfortunately, the Mössbauer data for **8** ( $\delta = 0.42$  mm/s,  $|\Delta E_{\text{Q}}| = 2.51$  mm/s, Table 2, Figure S16) fall in a range for which an unambiguous oxidation state and spin state assignment for the iron centre is not possible.<sup>11</sup>



Scheme 4. Synthesis of complex **8**.

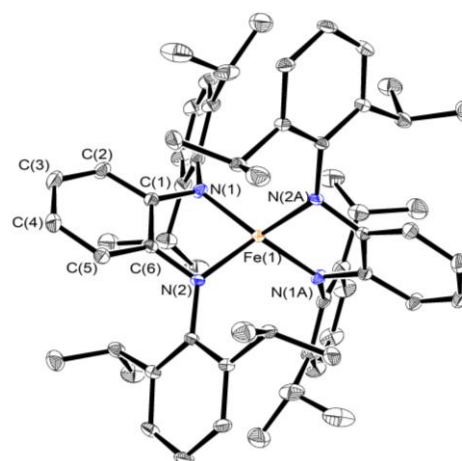


Figure 3. Molecular structure of **8** (30% probability thermal ellipsoids). All hydrogen atoms are omitted for clarity.

The structure of **8** was also examined with broken symmetry DFT calculations. The full structure of **8** was optimized into the same triplet ground state starting from various broken symmetry guesses, using PBEPBE<sup>13</sup> functionals and TZVP<sup>14</sup> basis set with Gaussian 16 software.<sup>15</sup> The optimized geometry closely resembles that of the crystal structure, as evidenced by the bond length data shown in Table 1. As shown in Figure 4, the spin density on Fe is 2.442, slightly lower than the expected value of an intermediate spin  $\text{Fe}(\text{III})$ , whereas the spin density of  $-0.442$  is fully delocalized over the two dpa ligands with significant spin density on the nitrogen donor atoms. Such a spin density distribution is consistent with the proposed electronic structure above, i.e., an intermediate spin  $\text{Fe}(\text{III})$  with significant



covalency and antiferromagnetic coupling between the metal centre and the two pda ligands.

TDDFT calculation was performed using PBEPB functionals and def2svp<sup>16</sup> basis set on the optimized structure from broken symmetry DFT calculation using the same functionals and basis set. The TDDFT simulated UV-Vis-NIR spectrum matches well with the experimental spectrum in terms of the wavelength of the absorption but not the intensity (Figure S21), which is expected. The frontier orbitals (Figures S22 and S23) and electronic transitions responsible for the low energy absorption bands are listed in Table S3. Due to the involvement of multiple transitions in each excited state and the mixed metal and ligand contribution to each frontier orbital, it is difficult to classify the nature of the low-energy absorption bands.

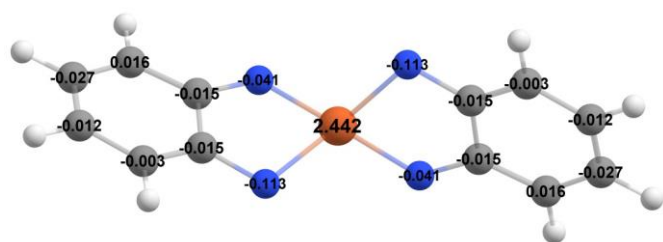
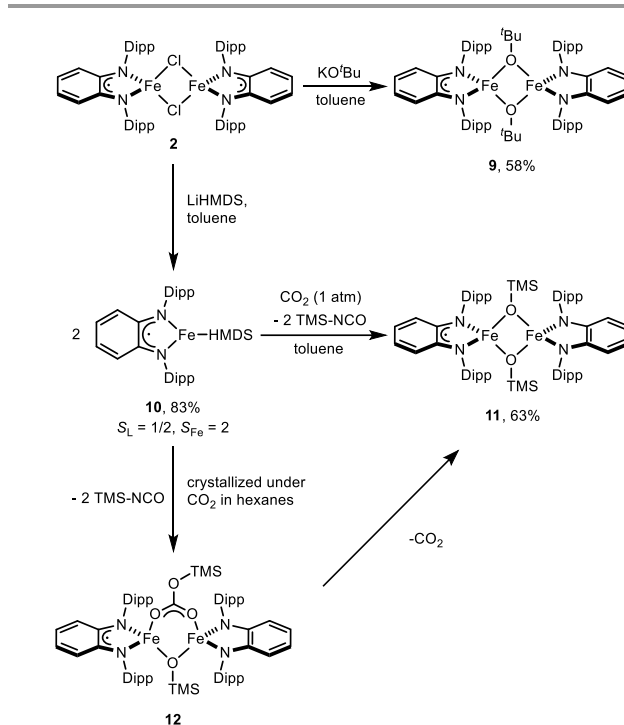


**Figure 4.** Computed spin density map for complex **8**. The Dipp groups on the pda ligands are omitted from this plot for clarity, although they were included in the calculation. Colour key: orange for Fe, blue for N, grey for C, and white for H.



**Scheme 5.** Syntheses of complexes **9–12**. The electronic structures of **9**, **11**, and **12** are ambiguous with available data; the tentative drawings of these compounds are just to show that the two [Dipp<sub>2</sub>pda-Fe] fragments within each molecule are different.

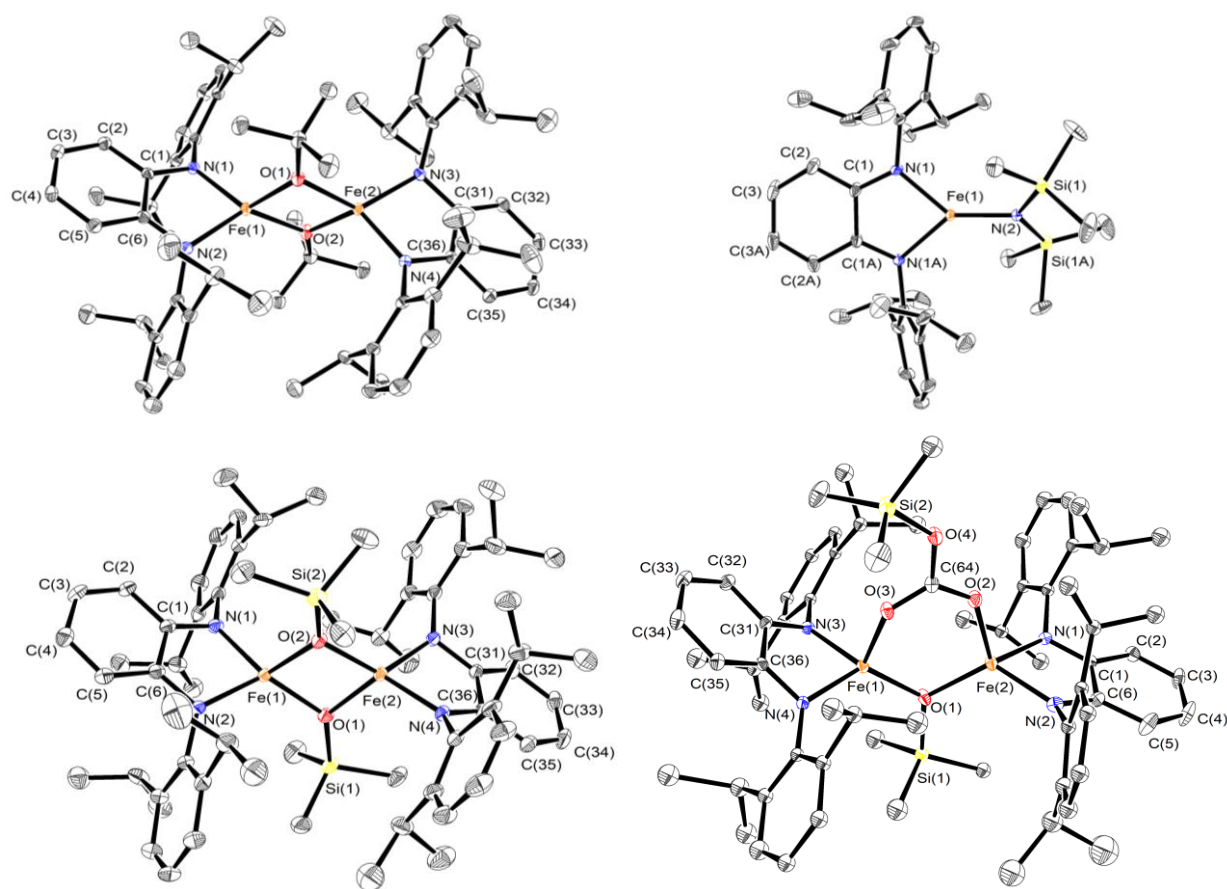


**Figure 5.** Molecular structure of **9–12** (30% probability thermal ellipsoids). All hydrogen atoms are omitted for clarity.



## ARTICLE

Exposing a toluene solution of **10** to 1 atm of CO<sub>2</sub> at room temperature results in the formation of TMS–NCO in a quantitative spectroscopic yield (with respect to complex **10**) within 30 minutes along with a mixture of new paramagnetic species, from which complex **11** can be isolated via recrystallization (Scheme 5). Metal silylamides have been reported to react with CO<sub>2</sub> to give isocyanates,<sup>18–20</sup> carbodiimides<sup>21</sup> and metal isocyanato complexes<sup>22</sup> along with the corresponding silyl ethers, metal siloxides or unidentified species. However, only a few reports show high selectivity towards the isocyanate under mild conditions,<sup>19</sup> as the resulting metal silyloxy species can further react with CO<sub>2</sub> or isocyanate product (isoelectronic with CO<sub>2</sub>) to carbodiimide or metal isocyanate and silyl ether.

In the solid-state, complex **11** has a dinuclear structure with two bridging trimethylsiloxide ligands between two <sup>Dipp</sup>pda–Fe fragments (Figure 5), resembling the structure of **9**. One of the <sup>Dipp</sup>pda ligands in **11** displays two C<sub>α</sub>–N distances of 1.368(3) and 1.364(4) Å, respectively, whereas the other displays two C<sub>α</sub>–N distances of 1.393(4) and 1.375(3) Å, respectively (Table 1). The trend in the Fe–N bond lengths of **11** is also similar to that of **9**. The observed solution magnetic moment 5.9 μ<sub>B</sub> at 25 °C in C<sub>6</sub>D<sub>6</sub> (Table 2). The Mössbauer spectrum of **11** at 80 K displays similar pattern as that of **9** (Table 2, Figure S19), suggesting a slight difference in the oxidation states of the two iron centres. Once again, the Mössbauer data for **11** are in the range that does not allow for an unambiguous assignment of the oxidation state and spin state of the iron centres.<sup>11</sup>

When a saturated hexanes solution of **10** is exposed to 1 atm. of CO<sub>2</sub> at –35 °C, a few crystals of complex **12** were obtained (Scheme 5). The molecular structure of **12** features two iron centres bridged by a trimethylsilyl carbonate and a trimethylsiloxide. One <sup>Dipp</sup>pda ligand in complex **12** displays two C<sub>α</sub>–N distances of 1.338(5) and 1.335(5) Å, respectively, whereas the other 1.379(5) and 1.378(5) Å, respectively. The Fe–N bond lengths in **12** also have the same pattern as in **9** and **11**. A better quality X-ray structure is needed to elucidate the oxidation state of the <sup>Dipp</sup>pda ligand. Complex **12** has the longest intramolecular Fe–Fe distance (3.2620(8) Å) among all the dinuclear complexes in this work. Unfortunately, complex **12** readily loses CO<sub>2</sub> to form complex **11** under vacuum, which hampers the isolation and further characterizations. The formation of **12** can be rationalized as the insertion of CO<sub>2</sub> into the Fe–O bond of the *in situ* formed **11**. Although isocyanates tend to show similar reactivity as CO<sub>2</sub>, we observed no reaction between TMS–NCO and complex **11** produced in the reaction of **10** and CO<sub>2</sub>. The lack of reactivity is presumably due to the steric congestion around the iron centres.

**Table 2.** Solution Magnetic Moment at 298 K and Mössbauer data at 80 K.

Complex	μ <sub>eff</sub> <sup>a</sup>	δ, mm/s	ΔE <sub>Q</sub>  , mm/s
<b>2</b>	5.4	0.84	3.64
<b>3</b>	-	0.37	0.79
<b>4</b>	5.2	0.72	4.02
<b>5</b>	4.2	0.81	2.05
<b>6</b>	4.1	0.80	3.04
<b>7</b>	5.1	0.39	2.12
<b>8</b>	2.7	0.42	2.51
<b>9</b>	6.1	0.66	2.81
		0.54	2.59
<b>10</b>	4.1	0.55	0.79
		0.76	2.28
<b>11</b>	5.9	0.60	2.61

<sup>a</sup> Solution magnetic moment by Evans method.

## Conclusions

In summary, a series of iron *o*-phenylenediamide complexes were synthesized. Their electronic structures were investigated through spectroscopic methods, and X-ray crystallography. The dimeric complex **2** contains two high-spin ferrous ions and two π-radical monoanionic ligands <sup>Dipp</sup>pda<sup>•-</sup> with strong antiferromagnetic coupling within each Fe–<sup>Dipp</sup>pda pair. Complex **3** features a low-spin Fe(I) centre and a <sup>Dipp</sup>pda<sup>•-</sup> ligand, where the electronic structure of the Fe<sup>I</sup>–<sup>Dipp</sup>pda<sup>•-</sup> moiety can be manipulated with different auxiliary ligands on iron. On the other hand, the Fe<sup>II</sup>–<sup>Dipp</sup>pda<sup>•-</sup> moiety in complexes **2**, **5** and **6** is persistent with various combinations of chloride and pyridine ligand. Such a phenomenon can be attributed to the low reducing power of the <sup>Dipp</sup>pda<sup>•-</sup> ligand. This hypothesis is consistent with the fact that 1e<sup>-</sup> oxidation of complex **6** gives Fe<sup>III</sup>–<sup>Dipp</sup>pda<sup>•-</sup> (rather than Fe<sup>II</sup>–<sup>Dipp</sup>pda<sup>0</sup>) moiety in **7**. Complex **8** with two bulky <sup>Dipp</sup>pda ligands on one iron centre is tentatively assigned as [Fe<sup>III</sup>(<sup>Dipp</sup>pda<sup>•-</sup>)(<sup>Dipp</sup>pda<sup>2-</sup>)] ↔ [Fe<sup>III</sup>(<sup>Dipp</sup>pda<sup>2-</sup>)(<sup>Dipp</sup>pda<sup>•-</sup>)], where the metal is antiferromagnetically coupled to the fully delocalized ligand-based radical based on literature precedence and available data. Using a bulky anionic ligand HMDS to replace the bridging chloride in **2**, we were able to obtain a mononuclear three-coordinate iron complex **9**, which shows reactivity toward CO<sub>2</sub> to give the trimethylsiloxide-bridge dimeric complex **11** and TMS–NCO selectively. Complex **11** can selectively react with CO<sub>2</sub> over the bulkier TMS–NCO in a reversible fashion to give complex **12**. Further investigation of the potential catalytic activities of these iron complexes are underway in our laboratories.



## Experimental Section

### General considerations

All reactions were carried out in a dinitrogen-filled glovebox or using the standard Schlenk techniques under dinitrogen. Glassware was dried in a 180 °C oven overnight. Diethyl ether, hexanes, pentane, and toluene solvents were dried by a Grubbs-type solvent purification system manufactured by Innovative Technology and degassed prior to use. THF solvent was dried by refluxing and distilling over sodium benzophenone ketyl under dinitrogen. Pyridine and hexamethyldisiloxane (HMDSO) were dried by refluxing and distilling over calcium hydride under dinitrogen. C<sub>6</sub>D<sub>6</sub>, and THF-*d*<sub>8</sub> were degassed through three consecutive freeze-pump-thaw cycles. All solvents were stored over 3 Å molecular sieves prior to use. Unless otherwise noted, all NMR spectra were recorded on an Agilent DD2 600 MHz spectrometer at 25 °C. Chemical shifts are referenced to the solvent signals. Solution magnetic moments were measured at 25 °C by the method originally described by Evans with stock and experimental solutions containing a known amount of a cyclohexane standard.<sup>23</sup> Elemental analyses were carried out by ANALEST at the University of Toronto. Electronic spectra were recorded with a Perkin-Elmer double-beam UV-VIS-NIR spectrometer Lambda 1050. All commercially available chemicals were used as received. Fe(HMDS)<sub>2</sub>Cl(THF),<sup>24</sup> and **1**<sup>25</sup> were prepared according to literature procedures. The <sup>1</sup>H NMR data are reported as chemical shift with the peak width at half-height in Hz, integration value, and partial assignment based on integration given in parentheses sequentially.

**<sup>57</sup>Fe Mössbauer Spectroscopy.** All measurements for <sup>57</sup>Fe Mössbauer spectroscopy were performed using non-enriched solids of the as-isolated complexes. All samples were prepared in an inert atmosphere glovebox equipped with a liquid nitrogen fill port to enable sample freezing to 77 K within the glovebox. Each sample was loaded into a Delrin Mössbauer sample cup for measurements and loaded under liquid nitrogen. Low temperature <sup>57</sup>Fe Mössbauer measurements were performed using a See Co. MS4 Mössbauer spectrometer integrated with a Janis SVT-400T He/N<sub>2</sub> cryostat for measurements at 80 K. Isomer shifts were determined relative to α-Fe at 298 K. All Mössbauer spectra were fit using the program WMoss (SeeCo). Errors of the fit analyses were the following: δ ± 0.02 mm/s and ΔE<sub>Q</sub> ± 3%. For multicomponent fits, the quantitation errors were ± 3% (e.g., 50 ± 3%).

**2:** To the mixture of **1** (857.3 mg, 2.00 mmol) and Fe(HMDS)<sub>2</sub>Cl(THF) (968.3 mg, 2.00 mmol) was added 10 mL of toluene. The reaction mixture was allowed to stir at 120 °C overnight. The reaction mixture changed from dark red to dark green. After cooling to room temperature, the reaction mixture was filtered through Celite. Volatiles were removed under vacuum, leaving a dark green solid. The solid was stirred with 10 mL of hexanes for 1 hour then collected on a frit, which was washed with hexanes (3 × 1 mL) and dried under high vacuum (882.4 mg, 85%). Crystals suitable for X-ray crystallography were obtained by cooling a concentrated diethyl ether solution

at -35 °C. <sup>1</sup>H NMR (600 MHz, C<sub>6</sub>D<sub>6</sub>) δ 158.25 (33.53, 4H), 67.20 (36.53, 4H), 2.02 (13.48, 24H, Dipp-CH<sub>3</sub>), -5.17 (207.12, 8H), -8.44 (8.85, 4H), -8.46 (7.39, 4H), -11.35 (9.73, 4H), -14.63 (28.63, 24H, Dipp-CH<sub>3</sub>). Evans method (298 K, C<sub>6</sub>D<sub>6</sub>): μ<sub>eff</sub> = 5.4 μ<sub>B</sub>. Anal. Calcd for C<sub>60</sub>H<sub>76</sub>N<sub>4</sub>Cl<sub>2</sub>Fe<sub>2</sub>·(C<sub>4</sub>H<sub>10</sub>O): C, 69.25; H, 7.81; N, 5.05. Found: C, 68.85; H, 7.48; N, 5.41.

**3:** To a 20 mL vial containing Hg (1.45 g) and 5 mL of toluene was added sodium metal (7.2 mg, 0.31 mmol). After stirring the resulting amalgam for 30 min, a solution of **2** (147.5 mg, 0.14 mmol) in 5 mL of toluene was added. The reaction mixture was stirred for 24 hours, then decanted and filtered through Celite. The filtrate was concentrated to dryness under vacuum. The solid residue was recrystallized from hexanes to afford metallic green crystals of **3** (132.7 mg, 82%). NMR data obtained are identical to those previously reported.<sup>7g</sup>

**4:** To a stirring solution of **3** (287.3 mg, 0.50 mmol) in 10 mL of THF was added pyridine (89 μL, 1.10 mmol). The reaction mixture was allowed to stir at room temperature overnight, and then filtered over Celite. The filtrate was concentrated to ~1 mL, top-layered with 5 mL of pentane and cooled to -35 °C overnight to yield dark blue purple crystals. The supernatant was decanted off, and the solid was washed with cold pentane (3 × 1 mL) and then dried under vacuum (212.3 mg, 66%). Crystals suitable for X-ray crystallography were obtained from cooling a concentrated diethyl ether solution at -35 °C. <sup>1</sup>H NMR (600 MHz, THF-*d*<sub>8</sub>) δ 118.39 (3921.27, 2H), 42.13 (31.48, 4H), 29.07 (238.34, 4H), 14.76 (156.00, 4H), 14.05 (710.18, 2H), 5.29 (37.32, 12H, Dipp-CH<sub>3</sub>), 0.28 (114.16, 12H, Dipp-CH<sub>3</sub>), -17.90 (40.82, 2H), -32.56 (123.98, 2H), -36.47 (26.66, 2H). Evans method (298 K, THF-*d*<sub>8</sub>): μ<sub>eff</sub> = 5.2 μ<sub>B</sub>. Anal. Calcd for C<sub>40</sub>H<sub>48</sub>N<sub>4</sub>Fe·(C<sub>4</sub>H<sub>8</sub>O): C, 74.14; H, 7.92; N, 7.86. Found: C, 74.52; H, 7.70; N, 8.13.

**5:** To a stirring solution of **2** (259.0 mg, 0.25 mmol) in 10 mL of toluene was added pyridine (50 μL, 0.63 mmol). The reaction mixture was allowed to stir at room temperature overnight, and then concentrated to dryness under vacuum. The residue was extracted into diethyl ether, filtered over Celite and slowly concentrated to ~2 mL. Top-layering with 5 mL of pentane and cooling to -35 °C overnight yielded green microcrystalline solid. The supernatant was decanted off, and the solid was washed with cold pentane (3 × 1 mL) and then dried under vacuum (218.4 mg, 73%). <sup>1</sup>H NMR (600 MHz, C<sub>6</sub>D<sub>6</sub>) δ 162.94 (1558.36, 1H), 104.68 (1394.75, 1H), 59.36 (1711.85, 1H), 34.19 (148.48, 2H), 2.63 (637.74, 12H, Dipp-CH<sub>3</sub>), -8.42 (96.38, 1H), -15.24 (290.19, 12H, Dipp-CH<sub>3</sub>), -28.15 (684.49, 2H). Evans method (298 K, C<sub>6</sub>D<sub>6</sub>): μ<sub>eff</sub> = 4.2 μ<sub>B</sub>. Anal. Calcd for C<sub>35</sub>H<sub>43</sub>N<sub>3</sub>FeCl: C, 70.41; H, 7.26; N, 7.04. Found: C, 70.07; H, 7.61; N, 7.20.

**6:** To a solid mixture of **2** (259.0 mg, 0.25 mmol) and tetrabutylammonium chloride (347.4 mg, 1.25 mmol) was added 10 mL of toluene. The reaction mixture was allowed to stir at room temperature overnight, and then filter through Celite. The filtrate was concentrated to ~1 mL, top-layered with 5 mL of hexanes and cooled to -35 °C overnight to afford blue

purple crystals. The supernatant was decanted off, and the solid was washed with hexanes (3 × 1 mL) and then dried under vacuum (319.2 mg, 80%). Crystals suitable for X-ray crystallography were obtained from vapor diffusion of pentane into its toluene solution at room temperature. <sup>1</sup>H NMR (600 MHz, C<sub>6</sub>D<sub>6</sub>) δ 161.99 (165.36, 1H), 70.63 (138.71, 1H), 12.70 (103.26, 8H), 7.37 (57.54, 8H), 2.44 (43.08, 8H), 1.14 (30.45, 12H), 0.58 (20.98, 12H, Dipp-CH<sub>3</sub>), 0.05 (34.41, 8H), -7.76 (69.52, 12H, Dipp-CH<sub>3</sub>), -25.24 (22.36, 2H). Evans method (298 K, C<sub>6</sub>D<sub>6</sub>): μ<sub>eff</sub> = 4.1 μ<sub>B</sub>. Anal. Calcd for C<sub>46</sub>H<sub>74</sub>N<sub>3</sub>Cl<sub>2</sub>Fe: C, 69.42; H, 9.37; N, 5.28. Found: C, 69.82; H, 9.62; N, 5.17.

**7:** In the absence of light, silver tetrafluoroborate (53.5 mg, 0.28 mmol) was added to a stirring solution of **6** (199.0 mg, 0.25 mmol) in 10 mL of toluene. The reaction mixture was allowed to stir at room temperature overnight, and then filter through Celite. The filtrate was concentrated to dryness. The residue was dissolved in toluene and filtered through Celite again, then concentrated ~1 mL, top-layered with 5 mL of pentane and cooled to -35 °C overnight to afford dark green microcrystalline solid. The supernatant was decanted off, and the solid was washed with pentane (3 × 1 mL) and then dried under vacuum (99.2 mg, 72%). Crystals suitable for X-ray crystallography were obtained from cooling a concentrated diethyl ether solution at -35 °C. <sup>1</sup>H NMR (600 MHz, C<sub>6</sub>D<sub>6</sub>) δ 218.94 (1083.40, 1H), 17.12 (175.98, 4H), 6.85 (570.77, 2H, overlap with C<sub>6</sub>D<sub>6</sub>), 0.95 (566.66, 12H, Dipp-CH<sub>3</sub>), -1.30 (212.26, 12H, Dipp-CH<sub>3</sub>), -37.18 (176.00, 2H). Evans method (298 K, C<sub>6</sub>D<sub>6</sub>): μ<sub>eff</sub> = 5.1 μ<sub>B</sub>. Anal. Calcd for C<sub>30</sub>H<sub>38</sub>N<sub>2</sub>Cl<sub>2</sub>Fe·0.6(C<sub>7</sub>H<sub>8</sub>): C, 67.49; H, 7.09; N, 4.60. Found: C, 67.55; H, 7.10; N, 4.66.

**8:** To a solution of **1** (535.8 mg, 1.25 mmol) in 5 mL of THF was slowly added <sup>n</sup>BuLi (2.5 M in hexanes, 1.00 mL, 2.50 mmol) at -80 °C. The resulting mixture was allowed to warm to room temperature slowly and further stirred for 2 h. The resulting suspension was cooled to -80 °C and a pre-cooled (-80 °C) slurry of anhydrous FeCl<sub>2</sub> (79.2 mg, 0.63 mmol, in 10 mL of THF) was added. The resulting mixture was allowed to warm to room temperature slowly and further stirred for 2 h, during which time the colour changed to dark purple. The mixture was cooled to -35 °C and a pre-cooled (-35 °C) solution of FeCl<sub>3</sub> (202.8 mg, 1.25 mmol, in 10 mL of THF) was added. The reaction mixture was stirred overnight, with a colour changed from dark purple to dark green. All volatiles were removed under vacuum, the residue was extracted into pentane and filtered through Celite. The filtrate was concentrated to ~5 mL, top-layered with 3 mL of HMDSO and cooled to -35 °C overnight to yield X-ray quality dark green crystals. The supernatant was decanted off, and the solid was washed with HMDSO (3 × 1 mL) and then dried under vacuum (445.6 mg, 78%). <sup>1</sup>H NMR (600 MHz, C<sub>6</sub>D<sub>6</sub>) δ 66.12 (117.84, 4H), 22.44 (36.62, 4H), 14.40 (25.23, 4H), 9.21 (223.83, 4H), 6.15 (531.51, 2H), 4.27 (23.57, 12H, Dipp-CH<sub>3</sub>), 3.92 (19.07, 12H, Dipp-CH<sub>3</sub>), -0.63 (22.96, 12H, Dipp-CH<sub>3</sub>), -2.82 (46.64, 12H, Dipp-CH<sub>3</sub>), -3.70 (124.70, 4H), -12.45 (35.67, 4H). Evans method (298 K, C<sub>6</sub>D<sub>6</sub>): μ<sub>eff</sub> = 2.7 μ<sub>B</sub>. Anal. Calcd for C<sub>60</sub>H<sub>76</sub>N<sub>4</sub>Fe·0.13(C<sub>6</sub>H<sub>18</sub>Si<sub>2</sub>O): C, 78.48; H, 8.49; N, 6.02. Found: C, 78.89; H, 8.65; N, 5.61.

**9:** To a stirring solution of **2** (259.0 mg, 0.25 mmol) in toluene was added KO<sup>t</sup>Bu (56.1 mg, 0.50 mmol) in toluene. The reaction mixture was allowed to stir at room temperature overnight, and then filtered through Celite. The filtrate was concentrated to ~1 mL, top-layered with 3 mL of pentane and cooled to -35 °C overnight to yield X-ray quality dark blue purple crystals. which was washed with pentane (5 × 1 mL) and dried under high vacuum (162.2 mg, 58%). <sup>1</sup>H NMR (600 MHz, C<sub>6</sub>D<sub>6</sub>) δ 45.56 (277.82, 4H), 40.71 (268.15, 4H), 26.80 (522.61, 4H), 13.94 (282.00, 12H, Dipp-CH<sub>3</sub>), 8.72 (442.06, 18H, OC(CH<sub>3</sub>)<sub>3</sub>), 3.54 (311.05, 12H), 1.26 (135.57, 12H, Dipp-CH<sub>3</sub>), -4.40 (909.99, 2H), -9.30 (314.89, 12H, Dipp-CH<sub>3</sub>), -19.68 (89.56, 4H), -31.60 (50.38, 4H), -35.93 (136.64, 4H). Evans method (298 K, C<sub>6</sub>D<sub>6</sub>): μ<sub>eff</sub> = 6.1 μ<sub>B</sub>. Anal. Calcd for C<sub>68</sub>H<sub>94</sub>N<sub>4</sub>O<sub>2</sub>Fe<sub>2</sub>·(C<sub>7</sub>H<sub>8</sub>): C, 74.86; H, 8.54; N, 4.66. Found: C, 74.74; H, 8.56; N, 4.56.

**10:** To a stirring solution of **2** (259.0 mg, 0.25 mmol) in toluene was added LiHMDS (83.7 mg, 0.5 mmol) in toluene. The reaction mixture was allowed to stir at room temperature overnight, and then concentrated to dryness under vacuum. The residue was extracted into pentane, filtered over Celite and slowly concentrated to dryness to afford a green brown microcrystalline solid, which was washed with cold pentane (3 × 0.5 mL) and dried under high vacuum (266.0 mg, 83%). Crystals suitable for X-ray crystallography were obtained from top-layering the pentane solution with HMDSO at -35 °C. <sup>1</sup>H NMR (600 MHz, C<sub>6</sub>D<sub>6</sub>) δ 266.68 (450.23, 1H), 130.82 (406.15, 2H), 11.91 (403.82, 18H, HMDS-CH<sub>3</sub>), 2.64 (105.35, 12H, Dipp-CH<sub>3</sub>), -20.20 (24.83, 2H), -27.94 (44.09, 4H), -38.61 (145.59, 12H), -88.02 (1824.32, 2H). Evans method (298 K, C<sub>6</sub>D<sub>6</sub>): μ<sub>eff</sub> = 4.1 μ<sub>B</sub>. Anal. Calcd for C<sub>36</sub>H<sub>56</sub>N<sub>3</sub>Si<sub>2</sub>Fe: C, 67.26; H, 8.78; N, 6.54. Found: C, 66.70; H, 8.81; N, 6.44.

**11:** A solution of **10** (160.7 mg, 0.25 mmol) in 10 mL of toluene was subjected to a freeze-pump-thaw cycle before 1 atm of CO<sub>2</sub> was introduced into the flask. The mixture was allowed to stir for 1 hour at room temperature, where the colour changed from green brown to dark blue. The reaction mixture was filtered through Celite. The filtrate was concentrated to ~1 mL, top-layered with 3 mL of pentane and cooled to -35 °C overnight to yield dark blue purple crystalline solid, which was washed with pentane (5 × 1 mL) and dried under high vacuum (89.8 mg, 63%). Crystals suitable for X-ray crystallography were obtained from cooling a concentrated diethyl ether solution at -35 °C. <sup>1</sup>H NMR (600 MHz, C<sub>6</sub>D<sub>6</sub>) δ 49.40 (279.92, 4H), 34.03 (43.46, 4H), 28.04 (42.69, 4H), 23.95 (69.80, 4H), 19.92 (43.02, 12H, Dipp-CH<sub>3</sub>), -0.50 (47.15, 12H, Dipp-CH<sub>3</sub>), -6.97 (7.63, 4H), -12.00 (390.53, 18H, OSi(CH<sub>3</sub>)<sub>3</sub>), -21.34 (74.98, 12H, Dipp-CH<sub>3</sub>), -27.06 (30.93, 4H), -31.35 (283.53, 4H). Evans method (298 K, C<sub>6</sub>D<sub>6</sub>): μ<sub>eff</sub> = 5.9 μ<sub>B</sub>. Anal. Calcd for C<sub>66</sub>H<sub>94</sub>N<sub>4</sub>O<sub>2</sub>Si<sub>2</sub>Fe<sub>2</sub>: C, 69.33; H, 8.29; N, 4.90. Found: C, 69.44; H, 8.78; N, 4.63.

## Conflicts of interest

There are no conflicts to declare.

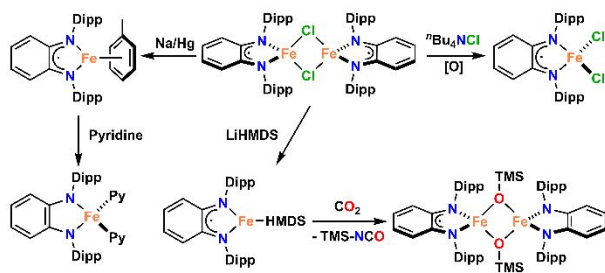
## Acknowledgements

We thank Natural Science and Engineering Research Council (NSERC) of Canada (grants to D.S.) and the National Science Foundation (CHE-1954480 to M.L.N.) for funding. Q.L. thanks the Ontario government for an Ontario Graduate Scholarship. J.H.L. thanks NSERC of Canada for a USRA. We also acknowledge the Ontario Research Fund for funding the CSICOMP NMR lab at the University of Toronto enabling the purchase of several new NMR spectrometers.

## Notes and references

- (a) A. Chirila, B. G. Das, P. F. Kuijpers, V. Sinha and B. de Bruin, in *Non-Noble Metal Catalysis: Molecular Approaches and Reactions*, ed. R. J. M. K. Gebbink and M.-E. Moret, Wiley-VCH, Weinheim, Germany, 2019, p. 1–31. (b) B. de Bruin, P. Gualco and N. D. Paul, in *Ligand Design in Metal Chemistry*, ed. M. Stradiotto and R. J. Lundgren, John Wiley & Sons, Ltd, Chichester, UK, 2016, p. 176–204; (c) J. I. van der Vlugt *Chem. Eur. J.*, 2019, **25**, 2651; (d) J. Jacquet, M. Desage-El Murr and L. Fensterbank, *ChemCatChem*, 2016, **8**, 3310; (e) A. I. Olivos Suarez, V. Lyaskovskyy, J. N. H. Reek, J. I. van der Vlugt and B. de Bruin, *Angew. Chem. Int. Ed.*, 2013, **52**, 12510; (f) O. R. Luca and R. H. Crabtree, *Chem. Soc. Rev.*, 2013, **42**, 1440; (h) R. F. Munhá, R. A. Zarkesh and A. F. Heyduk, *Dalton Trans.*, 2013, **42**, 3751; (o) V. Lyaskovskyy and B. de Bruin, *ACS Catal.*, 2012, **2**, 270; (j) K. G. Caulton, *Eur. J. Inorg. Chem.*, 2012, 435. (k) V. K. K. Praneeth, M. R. Ringenberg and T. R. Ward, *Angew. Chem. Int. Ed.*, 2012, **51**, 10228; (l) W. Kaim, *Eur. J. Inorg. Chem.*, 2012, 343; (m) P. J. Chirik, *Inorg. Chem.*, 2011, **50**, 9737; (n) P. J. Chirik and K. Wieghardt, *Science*, 2010, **327**, 794.
- (a) S. M. Rummelt, H. Zhong, I. Korobkov and P. J. Chirik *J. Am. Chem. Soc.*, 2018, **140**, 11589; (b) M. J. T. Wilding, D. A. Iovan, A. T. Wrobel, J. T. Lukens, S. N. MacMillan, K. M. Lancaster and T. A. Betley, *J. Am. Chem. Soc.*, 2017, **139**, 14757; (c) W. J. T. Wilding, D. A. Iovan and T. A. Betley, *J. Am. Chem. Soc.*, 2017, **139**, 12043.
- (a) J. M. Hoyt, V. A. Schmidt, A. M. Tondreau and P. J. Chirik *Science*, 2015, **349**, 960; (b) A. M. Tondreau, C. C. H. Atienza, K. J. Weller, S. A. Nye, K. M. Lewis, J. G. P. Delis and P. J. Chirik, *Science*, 2012, **335**, 567. (c) D. A. Iovan, M. J. T. Wilding, Y. Baek, E. T. Hennessy and T. A. Betley, *Angew. Chem. Int. Ed.*, 2017, **56**, 15599; (d) E. T. Hennessy and T. A. Betley, *Science*, 2013, **340**, 591.
- (a) C. G. Pierpont, *Coord. Chem. Rev.*, 2001, **216–217**, 99; (b) D. L. J. Broere, R. Plessius and J. I. van der Vlugt, *Chem. Soc. Rev.*, 2015, **44**, 6886.
- (a) M. V. Joannou, M. J. Bezdek, K. Albahily, I. Korobkov and P. J. Chirik *Organometallics* 2018, **37**, 3389; (b) M. J. Sgro and D. W. Stephan *Dalton Trans.*, 2010, **39**, 5786; (c) W. W. Kramer, L. A. Cameron, R. A. Zarkesh, J. W. Ziller and A. F. Heyduk *Inorg. Chem.* 2014, **53**, 8825; (d) N. G. Léonard and P. J. Chirik *ACS Catal.*, 2018, **8**, 342; (e) W. N. Palmer and P. J. Chirik *ACS Catal.*, 2017, **7**, 5674; (f) L. Pei, F. Liu, H. Liao, J. Gao, L. Zhong, H. Gao and Q. Wu *ACS Catal.*, 2018, **8**, 1104; (g) X.-J. Yang, X. Fan, Y. Zhao, X. Wang, B. Liu, J.-H. Su, Q. Dong, M. Xu and B. Wu *Organometallics*, 2013, **32**, 6945; (h) K. Y. Monakhov, J. van Leusen, P. Kögerler, E.-L. Zins, M. E. Alikhani, M. Tromp, A. A. Danopoulos and P. Braunstein *Chem. Eur. J.*, 2017, **23**, 6504; (i) M. van der Meer, Y. Rechkemmer, I. Peremykin, S. Hohloch, J. van Slageren and B. Sarkar *Chem. Commun.*, 2014, **50**, 1110; (j) H. Nishiyama, H. Ikeda, T. Saito, B. Kriegel, H. Tsurugi, J. Arnold and K. Mashima *J. Am. Chem. Soc.*, 2017, **139**, 6494; (k) J. Bendix and K. M. Clark, *Angew. Chem. Int. Ed.*, 2016, **55**, 2748; (l) T. Janes, M. Xu and D. Song, *Dalton Trans.*, 2016, **45**, 10672.
- (a) D. A. Evans and A. H. Cowley, *J. Am. Chem. Soc.*, 2012, **134**, 15672; (b) D. A. Evans, I. Vargas-Baca and A. H. Cowley, *J. Am. Chem. Soc.*, 2013, **135**, 13939; (c) I. L. Fedushkin, V. A. Dodonov, A. A. Skatova, V. G. Sokolov, A. V. Piskunov and G. K. Fukin, *Chem. Eur. J.*, 2018, **24**, 1877; (d) K. V. Vasudevan, M. Findlater, I. Vargas-Baca and A. H. Cowley *J. Am. Chem. Soc.*, 2012, **134**, 176; (e) Y. Segawa, Y. Suzuki, M. Yamashita and K. Nozaki, *J. Am. Chem. Soc.*, 2008, **130**, 16069; (f) K. L. Bamford, L. E. Longobardi, L. Liu, S. Grimme and D. W. Stephan, *Dalton Trans.*, 2017, **46**, 5308; (g) W. Zhang, V. A. Dodonov, W. Chen, Y. Zhao, A. A. Skatova, I. L. Fedushkin, P. W. Roesky, B. Wu and X.-J. Yang, *Chem. Eur. J.*, 2018, **24**, 14994; (h) T. Janes, P. Zatsepin and D. Song, *Chem. Commun.*, 2017, **53**, 3090; (n) M. Ma, L. Shen, H. Wang, Y. Zhao, B. Wu and X.-J. Yang, *Organometallics*, 2020, **39**, 1440; (m) Y. Liu, S. Li, X.-J. Yang, P. Yang and B. Wu, *J. Am. Chem. Soc.*, 2009, **131**, 4210.
- (a) S. C. Bart, E. J. Hawrelak, A. K. Schmisser, E. Lobkovsky and P. J. Chirik, *Organometallics*, 2004, **23**, 237; (b) N. Muresan, C. C. Lu, M. Ghosh, J. C. Peters, M. Abe, L. M. Henling, T. Weyhermüller, E. Bill and K. Wieghardt, *Inorg. Chem.*, 2008, **47**, 4579; (c) M. M. Khusniyarov, E. Bill, T. Weyhermüller, E. Bothe, K. Harms, J. Sundermeyer and K. Wieghardt, *Chem. Eur. J.*, 2008, **14**, 7608; (d) M. M. Khusniyarov, T. Weyhermüller, E. Bill and K. Wieghardt, *J. Am. Chem. Soc.*, 2009, **131**, 1208; (e) M. M. Khusniyarov, T. Weyhermüller, E. Bill and K. Wieghardt, *Angew. Chem. Int. Ed.*, 2008, **47**, 1228; (f) A. Hernán-Gámez, M. Rodríguez, T. Parella and M. Costas, *Angew. Chem. Int. Ed.*, 2019, **58**, 13904; (g) T. Janes, J. M. Rawson and D. Song, *Dalton Trans.*, 2013, **42**, 10640.
- (a) S. C. Bart, E. J. Hawrelak, E. Lobkovsky and P. J. Chirik, *Organometallics*, 2005, **24**, 5518; (b) V. A. Schmidt, C. R. Kennedy, M. J. Bezdek and P. J. Chirik, *J. Am. Chem. Soc.*, 2018, **140**, 3443; (c) H. tom Dieck and H. Bruder, *J. Chem. Soc., Chem. Commun.*, 1977, 24; (d) H. tom Dieck and J. Dietrich, *Angew. Chem. Int. Ed.*, 1985, **24**, 781; (e) P. Le Floch, F. Knoch, F. Kremer, F. Mathey, J. Scholz, W. Scholz, K.-H. Thiele and U. Zenneck, *Eur. J. Inorg. Chem.*, 1998, 119; (f) H. tom Dieck and R. Diercks, *Angew. Chem. Int. Ed.*, 1983, **22**, 778; (g) C. Lichtenberg, M. Adelhardt, T. L. Gianetti, K. Meyer, B. de Bruin and H. Grützmacher, *ACS Catal.*, 2015, **5**, 6230; (h) H. Lee, M. G. Campbell, R. H. Sánchez, J. Börgel, J. Raynaud, S. E. Parker and T. Ritter, *Organometallics*, 2016, **35**, 2923; (i) R. K. O'Reilly, M. P. Shaver, V. C. Gibson and A. J. P. White, *Macromolecules*, 2007, **40**, 7441; (j) C.-H. Ke, C.-H. Chen, M.-L. Tsai, H.-C. Wang, F.-T. Tsai, Y.-W. Chiang, W.-C. Shih, D. S. Bohle and W.-F. Liaw, *J. Am. Chem. Soc.*, 2017, **139**, 67.
- (a) M. Villa, D. Miesel, A. Hildebrandt, F. Ra-gaini, D. Schaarschmidt and A. Jacobi von Wangelin, *ChemCatChem* 2017, **9**, 3203; (b) A. Saini, C. R. Smith, F. S. Wekesa, A. K. Helms and M. Findlater *Org. Biomol. Chem.*, 2018, **16**, 9368; (c) X. Yu, F. Zhu, D. Bu and H. Lei *RSC Adv.*, 2017, **7**, 15321; (d) V. V. Khrizanforova, V. I. Morozov, M. N. Khrizanforov, A. N. Lukoyanov, O. N. Kataeva, I. L. Fedushkin and Yu. H. Budnikova, *Polyhedron*, 2018, **154**, 77; (e) P. J. Larson, F. S. Wekesa, A. Singh, C. R. Smith, A. Rajput, G. P. McGovern, D. K. Unruh, A. F. Cozzolino and M. Findlater, *Polyhedron*, 2018, **159**, 365; (f) A. Paulovicova, U. El-Ayaan, K. Umezawa, C. Vithana, Y. Ohashi and Y. Fukuda, *Inorg. Chim. Acta.*, 2002, **339**, 209; (g) D. A. Piryazev, M. A. Ogienko, A. V. Virovets, N. A. Pushkarevsky and S. N. Konchenko, *Acta Crystallogr. Sect. C* 2012, **68**, m320; (h) I. L. Fedushkin, A. A. Skatova, N. M. Khvoinova, A. N. Lukoyanov, G. K. Fukin, S. Y. Ketkov, M. O. Maslov, A. S. Bogomyakov and V. M. Makarov, *Russ. Chem. Bull.*, 2013, **62**, 2122; (i) M. Schmitz, M. Seibel, H. Kelm, S. Demeshko, F. Meyer and H.-J. Krüger, *Angew. Chem. Int. Ed.*, 2014, **53**, 5988; (j) F. S. Wekesa, R. Arias-Ugarte, L. Kong, Z. Sumner, G. P. McGovern and M. Findlater, *Organometallics*,

- 2015, **34**, 5051; (k) M. J. Supej, A. Volkov, L. Darko, R. A. West, J. M. Darmon, C. E. Schulz, K. A. Wheeler and H. M. Hoyt, *Polyhedron*, 2016, **114**, 403; (l) L. A. Brown, F. S. Wekesa, D. K. Unruh, M. Findlater and B. K. J. Long, *Polym. Sci., Part A: Polym. Chem.*, 2017, **55**, 2824.
- 10 W. P. Fehlhammer, H. Stolzenberg, in *Comprehensive Organometallic Chemistry*, ed. G. Wilkinson, F. G. A. Stone, F. W. Abel, Pergamon Press, Oxford, UK, 1982, p. 515-524.
- 11 P. Gütlich, E. Bill and A. X. Trautwein, *Mössbauer Spectroscopy and Transition Metal Chemistry. Fundamentals and Applications*, Springer, Berlin, Germany, 2011.
- 12 P. J. Hay, J. C. Thibeault, R. Hoffmann, *J. Am. Chem. Soc.* 1975, **97**, 4884.
- 13 J. P. Perdew, K. Burke, M. Ernzerhof, *Phys. Rev. Lett.* 1996, **77**, 3865.
- 14 A. Schäfer, C. Huber, R. Ahlrichs, *J. Chem. Phys.* 1994, **100**, 5829.
- 15 M. J. Frisch, G. W. Trucks, H. B. Schlegel, G. E. Scuseria, M. A. Robb, J. R. Cheeseman, G. Scalmani, V. Barone, G. A. Petersson, H. Nakatsuji, X. Li, M. Caricato, A. V. Marenich, J. Bloino, B. G. Janesko, R. Gomperts, B. Mennucci, H. P. Hratchian, J. V. Ortiz, A. F. Izmaylov, J. L. Sonnenberg, D. Williams-Young, F. Ding, F. Lipparini, F. Egidi, J. Goings, B. Peng, A. Petrone, T. Henderson, D. Ranasinghe, V. G. Zakrzewski, J. Gao, N. Rega, G. Zheng, W. Liang, M. Hada, M. Ehara, K. Toyota, R. Fukuda, J. Hasegawa, M. Ishida, T. Nakajima, Y. Honda, O. Kitao, H. Nakai, T. Vreven, K. Throssell, J. A. Montgomery, Jr., J. E. Peralta, F. Ogliaro, M. J. Bearpark, J. J. Heyd, E. N. Brothers, K. N. Kudin, V. N. Staroverov, T. A. Keith, R. Kobayashi, J. Normand, K. Raghavachari, A. P. Rendell, J. C. Burant, S. S. Iyengar, J. Tomasi, M. Cossi, J. M. Millam, M. Klene, C. Adamo, R. Cammi, J. W. Ochterski, R. L. Martin, K. Morokuma, O. Farkas, J. B. Foresman, and D. J. Fox, Gaussian, Inc., Wallingford CT, 2016.
- 16 F. Weigend, R. Ahlrichs, *Phys. Chem. Chem. Phys.* 2005, **7**, 3297.
- 17 (a) H. Andres, E. L. Bominaar, J. M. Smith, N. A. Eckert, P. L. Holland, E. Münck, *J. Am. Chem. Soc.* **2002**, *124*, 3012; (b) S. Yogendra, T. Weyhermüller, A. W. Hahn, S. DeBeer, *Inorg. Chem.* **2019**, *58*, 9358.
- 18 (a) M. Reiter, S. Vagin, A. Kronast, C. Jandl, B. Rieger, *Chem. Sci.* 2017, **8**, 1876; (b) D. R. Moore, M. Cheng, E. B. Lobkovsky, G. W. Coates, *J. Am. Chem. Soc.* 2003, **125**, 11911.
- 19 (a) D. A. Dickie, K. B. Gislason, R. A. Kemp, *Inorg. Chem.* 2012, **51**, 1162; (b) A. M. Felix, B. J. Boro, D. A. Dickie, Y. Tang, J. A. Saria, B. Moasser, C. A. Stewart, B. J. Frost, R. A. Kemp, *Main Group Chem.* 2012, **11**, 13; (c) M. Xu, A. R. Jupp, D. W. Stephan, *Angew. Chem. Int. Ed.*, 2017, **56**, 14277; (d) D. L. J. Broere, B. Q. Mercado, P. L. Holland, *Angew. Chem. Int. Ed.*, 2018, **57**, 6507.
- 20 H. Yin, P. J. Carroll, E. J. Schelter, *Chem. Commun.* 2016, **52**, 9813.
- 21 L. R. Sita, J. R. Babcock, R. Xi, *J. Am. Chem. Soc.* 1996, **118**, 10912.
- 22 (a) C. Camp, L. Chatelain, C. E. Kefalidis, J. Pécaut, L. Maron, M. Mazzanti, *Chem. Commun.* 2015, **51**, 15454; (b) M. T. Whited, A. J. Kosanovich, D. E. Janzen, *Organometallics* 2014, **33**, 1416; (c) P. Arnold, Z. R. Turner, A. I. Germeroth, I. J. Casely, G. S. Nichol, R. Bellabarba, R. P. Tooze, *Dalton Trans.* 2013, **42**, 1333; (d) W. Sattler, G. Parkin, *J. Am. Chem. Soc.* 2011, **133**, 9708; (e) B. C. Fullmer, H. Fan, M. Pink, K. G. Caulton, *Inorg. Chem.* 2008, **47**, 1865; (f) H. Phull, D. Alberti, A. L. Korobkov, S. Gambarotta, P. H. M. Budzelaar, *Angew. Chem. Int. Ed.* 2006, **45**, 5331.
- 23 D. F. Evans, *J. Chem. Soc.*, 1959, 2003.
- 24 J. S. Duncan, T. M. Nazif, A. K. Verma and S. C. Lee, *Inorg. Chem.*, 2003, **42**, 1211.
- 25 T. Wenderski, K. M. Light, D. Ogrin, S. G. Bott and C. J. Harlan, *Tetrahedron Lett.*, 2004, **45**, 6851.



We report the reactivity of the iron complexes of a bulky phenylenediamide ligand.